Title	Experimental evidences of topological surface states of β-Ag2Te
Author(s)	Sulaev, A; Ren, P; Xia, B; Lin, QH; Yu, T; Qiu, CY; Zhang, SY; Han, MY; Li, ZP; Zhu, WG; Wu, QY; Feng, YP; Shen, L; Shen, S; Wang, L
Citation	AIP Advances, 2013, v. 3, p. 032123:1-12
Issued Date	2013
URL	http://hdl.handle.net/10722/183147
Rights	AIP Advances. Copyright © American Institute of Physics.

AIP ADVANCES **3**, 032123 (2013)

Experimental evidences of topological surface states of β-Ag_2Te

Azat Sulaev,[1,a] Peng Ren,[1,a] Bin Xia,[1] Qing Hua Lin,[1] Ting Yu,[1] Caiyu Qiu,[1] Shuang-Yuan Zhang,[2] Ming-Yong Han,[2] Zhi Peng Li,[3] Wei Guang Zhu,[3] Qingyu Wu,[4] Yuan Ping Feng,[4] Lei Shen,[4,b] Shun-Qing Shen,[5] and Lan Wang[1,b]

[1]*School of Physical and Mathematical Science, Nanyang Technological University, Singapore, 637371, Singapore*
[2]*Institute of Materials Research and Engineering, Singapore, 117602, Singapore*
[3]*School of Electrical and Electronic Engineering, Nanyang Technological University, Singapore, 639789, Singapore*
[4]*Department of Physics, National University of Singapore, Singapore*
[5]*Department of Physics, The University of Hong Kong, Pokfulam Road, Hong Kong, People's Republic of China*

(Received 20 December 2012; accepted 27 February 2013; published online 12 March 2013)

We present evidence of topological surface states in β-Ag_2Te through first-principles calculations, periodic quantum interference effect and ambipolar electric field effect in single crystalline nanoribbon. Our first-principles calculations show that β-Ag_2Te is a topological insulator with a gapless Dirac cone with strong anisotropy. To experimentally probe the topological surface state, we synthesized high quality β-Ag_2Te nanoribbons and performed electron transport measurements. The coexistence of pronounced Aharonov-Bohm oscillations and weak Altshuler-Aronov-Spivak oscillations clearly demonstrates coherent electron transport around the perimeter of β-Ag_2Te nanoribbon and therefore the existence of topological surface states, which is further supported by the ambipolar electric field effect for devices fabricated by β-Ag_2Te nanoribbons. The experimental evidences of topological surface states and the theoretically predicted anisotropic Dirac cone of β-Ag_2Te suggest that the material may be a promising candidate of topological insulator for fundamental study and future spintronic devices. [http://dx.doi.org/10.1063/1.4795735]

I. INTRODUCTION

Topological insulator is a state of quantum matter characterized by Z_2 invariance. It is composed of a fully filled insulating bulk state and an odd number of massless spin-helical Dirac cones of two-dimensional surface states.[1–3] Due to the fascinating new physics and great potential application in spintronics and quantum computation, topological insulator quickly becomes a trend research field in condensed matter physics. Various two- and three-dimensional topological insulator systems have been proposed via band structure calculation. However, up to date, only CdTe/HgTe/CdTe[4,5] and InAs/GaSb[6] quantum well structures have been experimentally confirmed to be two-dimensional topological insulator while strained HgTe[7,8] and several Bi based compounds, such as Bi_xSb_{1-x}, Bi_2Se_3, Bi_2Te_3, *etc*,[9–20] have been confirmed to be three-dimensional topological insulators. Thus, exploiting and identifying other good candidates of topological insulators with special characteristics is crucial and desirable.

[a]These authors contributed equally to this work.
[b]Authors to whom correspondence should addressed. Electronic mail: shenlei@nus.edu.sg, wanglan@ntu.edu.sg

β-Ag_2Te, a narrow band gap nonmagnetic semiconductor, shows unusual large and nonsaturating quasi-linear magnetoresistance in the field range of 10–10^5 Oe and the temperature range of 5–300 K.[21,22] The origin of the unusual magnetoresistance has generated debates since its discovery.[23–25] Recently, β-Ag_2Te was predicted to be a topological insulator with gapless Dirac-type surface states via band structure calculation.[26] It was proposed that the observed unusual magnetoresistance may largely come from the surface or interface contribution. The characteristic feature of this new binary topological insulator is a highly anisotropic Dirac cone. So far, the topological surface states of β-Ag_2Te and Bi_2Se_3 (221) surface[43] have been predicted to be highly anisotropic. Physical realization of topological insulator with highly anisotropic Dirac fermions may lead to a discovery of novel electronic states and long spin relaxation time in topological insulators.[27] The long spin relaxation time is extremely important for the application of topological insulator in spintronics, which has barely been studied so far.

In order to verify the essential features of the aforementioned picture, we utilized a different method to perform band structure calculations and carried out magnetotransport and gated electric transport experiments on single crystalline β-Ag_2Te nanoribbons. Our calculations confirmed the anisotropic topological surface state, although the shape of the surface state of our calculations is different from that in the literature.[26] The existence of the surface states in Ag_2Te is confirmed experimentally, based on the Aharonov-Bohm interference pattern obtained in the magnetotransport measurements at low temperatures. It is further supported by the ambipolar electric field effect for devices fabricated by β-Ag_2Te nanoribbons.

II. BAND STRUCTURE CALCULATION

Our density functional calculations were carried out using the Vienna *ab initio* simulation package (VASP)[28] with projector-augmented-wave potentials[29] and the Perdew-Burke-Ernzerhof generalized gradient approximation[30] for exchange-correlation functional. The Hamiltonian contained the scalar relativistic corrections and the spin-orbit coupling was taken into account by the second variation method.[31] The lattice constants of β-Ag_2Te were adopted from experiments.[32] The generic β-Ag_2Te substrate was modeled by a slab of 48 atomic layers or 12 unit cell layers along the hexagonal c-axis.[26] The slab calculations presented in this work were performed using symmetric setups, so the upper and lower surfaces were identical and their energy bands were degenerated. The vacuum layers were over 20 Å thick to ensure decoupling between neighboring slabs. The cutoff for plane-wave expansion was set to be 300 eV and a $7 \times 7 \times 1$ k-point mesh was used for the surface unit cell. In the band structure calculations of Zhang *et al.*,[26] first-principles calculations were utilized in the bulk state of β-Ag_2Te, while tight-binding method was employed to calculate the surface state. To keep the calculations consistently and improve the accuracy of description of the surface state, we used first principles calculations for both bulk and surface band-structure calculations.

Fig. 1 shows the calculated surface band structure of β-Ag_2Te with spin-orbital coupling (SOC) included and the out-of-plane of the surface is along the c-axis. The shaded area is the bulk band structure projected to the 2D Brillouin zone. It is seen that the bulk gap is around 0.1 eV which is in good agreement with experimental data.[33,34] The upper inset shows the shape of the 2D Brillouin zone for the surface unit cell. The red solid lines are the surface topological state, which show a single Dirac cone on the surface, which is similar to that obtained via tight binding method[26] although the shapes of the surface state are different. The bottom inset shows the constant-energy contours which cut through the surface state below the Dirac point at energies of −10 meV, −20 meV and −30 meV. The red (blue) color means the out-of-plane components pointing out-(in-) ward of the plane. The color scale, with blue and red, indicates the intensity of negative and positive values representing the projection S_z. Our results show that the spin direction of the surface states precesses counterclockwise around the Γ point below the Dirac point and has out-of-plane component. The most interesting phenomenon is the anisotropic surface Dirac cone of β-Ag_2Te which is different from the round and warped hexagonal surface state of Bi_2Se_3 and Bi_2Te_3.[10,35] It is because of the absence of the rotational symmetry in β-Ag_2Te.

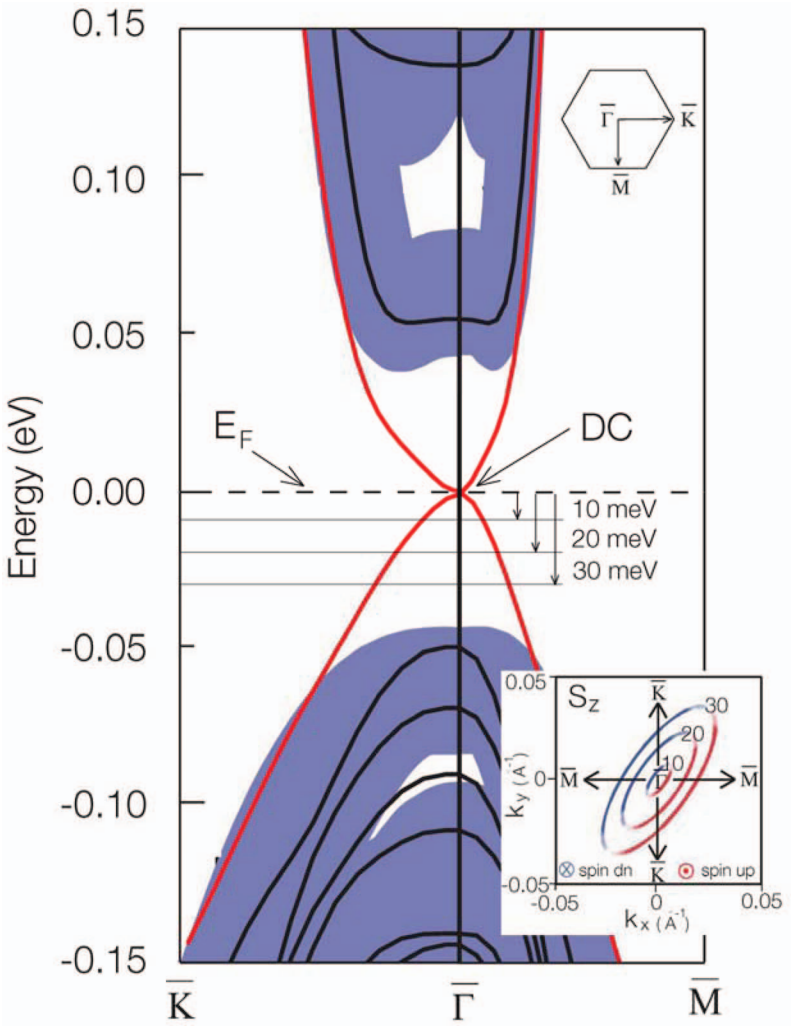

FIG. 1. The calculated surface band structure of the β-Ag_2Te film with the projected bulk band structure in the background (blue) to the 2D Brillouin zone whose shape is shown in the upper inset. The surface topological states are highlighted by the red lines. The bottom inset shows the expectation values of spin operator (S_z) of the surface band in β-Ag_2Te along k_x and k_y directions in momentum space. Three constant-energies, which cut through the surface state below the Dirac point, are plotted. The red (blue) color means the out-of-plane components pointing out-(in-) ward of the plane. The color scale, with blue and red, indicates the intensity of negative and positive values representing the projection S_z.

III. EXPERIMENT

Ag_2Te nanoribbons were synthesized by CVD method inside a 30 cm horizontal tube furnace equipped with a 3 cm diameter quartz tube.[36] The base pressure of the system was 3×10^{-7} torr. The powder of Ag_2Te (Sigma-Aldrich, 99.99%) was used as a precursor placed at the hot center region. Sapphire substrates were placed downstream 14–17 cm away from the hot center region without any catalyst. Before the usage, the substrates were cleaned using acid, ethanol and IPA. The tube was flushed three times with the argon gas to decrease oxygen contamination. The typical growth conditions for the nanoribbons are: 0.026g Ag_2Te, pressure 7.5 torr, source temperature 980°C, growth time 1 hour, and gas flow rate 50 s.c.c.m. Nanoribbons generally grow at the position range of 15–16 cm away from the center. As grown ribbons are typically 100–200 nm thick, 100 nm to several micrometers wide, and up to tens of micrometers long.

Transmission electron microscopy (TEM) images were examined by Philips CM300 field emission gun transmission electron microscope operating at an accelerated voltage of 300 kV. The

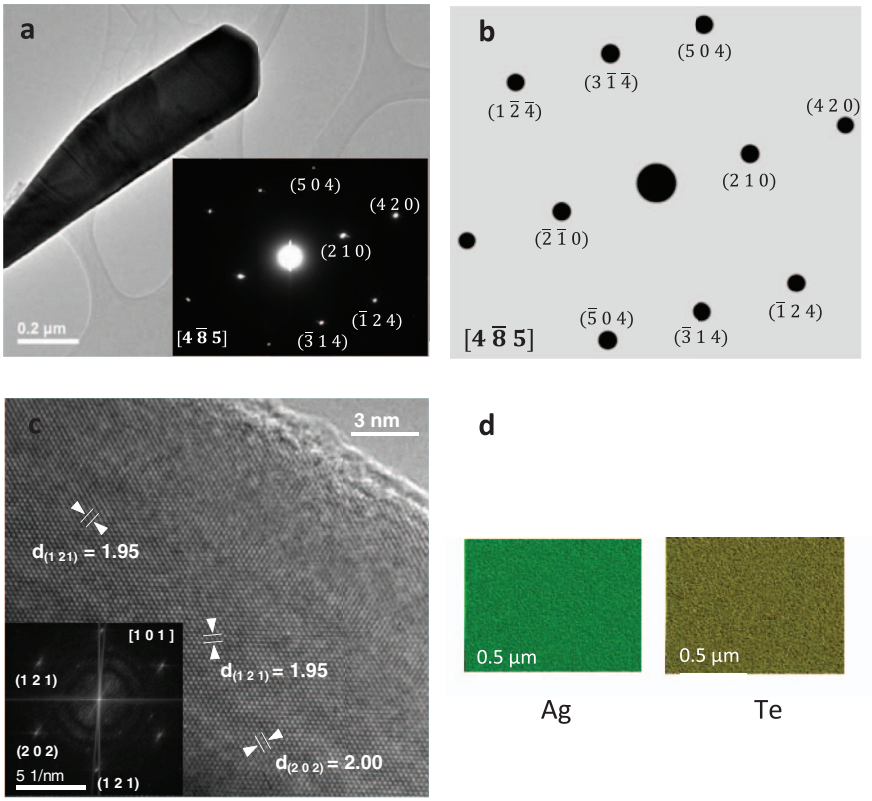

FIG. 2. (a) TEM image of an as prepared nanoribbon with the inset showing the corresponding SAED pattern. (b) Transmission electron diffraction pattern simulated based on monoclinic Ag_2Te single crystal with cell parameters $a = 8.164$ Å, $b = 4.468$ Å, $c = 8.977$ Å, space group $P2_1/c$ (ICSD file number: 073402). The electrons are directed to the sample at zone axis [4 $\bar{8}$5] with energy at 300 KeV. (c) High resolution TEM image of a focused ion beam milled Ag_2Te nanoribbon with the inset showing the corresponding fast Fourier transform pattern. (d) EDS mapping for Ag_2Te nanoribbon.

deposited nanoribbons on the sapphire substrate were placed in a vial containing 2 mL methanol solvent, and subsequently ultrasonicated for 10 min to separate the nanoribbons from substrate and disperse them into solvent. A drop of such dispersion (2μL) was withdrawn and added onto a carbon-coated copper grid, which was placed on a piece of tissue paper. The solvent on the copper grid was immediately adsorbed by the tissue paper and ready for the TEM characterization. The atomic ratio between Ag and Te was determined by energy-dispersive X-ray spectroscopy in a scanning electron microscopy. The width and thickness of the nanoribbons were determined by scanning electron microscopy and atomic force microscopy, respectively. The transmission electron microscopy (TEM) and corresponding selected area electron diffraction (SAED) investigation was carried out for the as-prepared nanoribbons. Fig. 2 shows a TEM image of nanoribbons. The diffraction pattern (Fig. 2(a) inset) shows clearly that the nanoribbon is single crystalline and matches well with the standard monoclinic β-Ag_2Te (ICSD file number: 073402) single crystal electron diffraction pattern (Fig. 2(b)) at zone axis [4 $\bar{8}$ 5]. The electron diffraction pattern are simulated based on monoclinic Ag_2Te single crystal with cell parameters $a = 8.164$ Å, $b = 4.468$ Å, $c = 8.977$ Å, space group $P2_1/c$. A high resolution TEM picture of focused ion beam milled β-Ag_2Te is shown in Fig. 2(c). It is clear from the picture and corresponding fast Fourier transform pattern that our single crystalline Ag_2Te is very high quality and the growth direction is perpendicular to the $(1\bar{2}1)$ plane direction. Energy-dispersive X-ray spectroscopy (EDS) shows that the atomic ratio of Ag and Te is 2.02 (with an error bar of ~0.5%) as shown in Fig. 3. The distribution of Ag and Te is homogeneous in the sample, as shown by the EDS mapping in Fig. 2(d). The transmission electron microscopy (TEM), corresponding selected area electron diffraction (SAED) and Energy-dispersive X-ray spectroscopy (EDS) demonstrate that high quality monoclinic β-Ag_2Te nanoribbons have been synthesized.

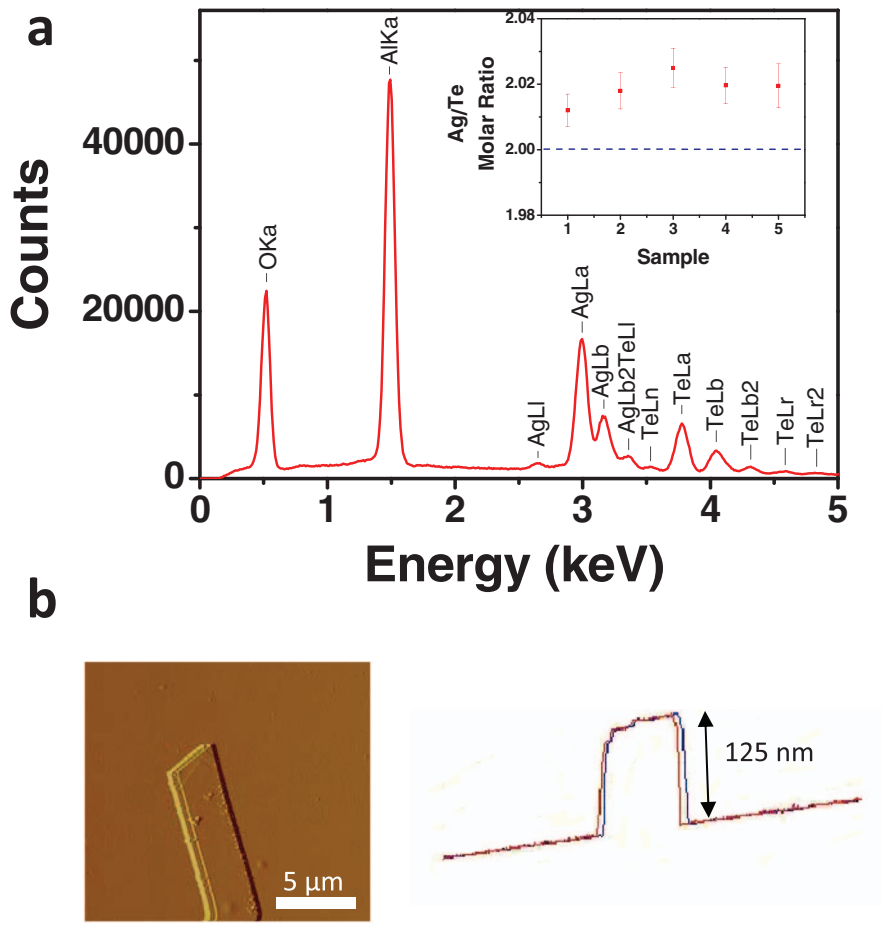

FIG. 3. (a) EDS spectrum of a Ag_2Te nanoribbon. Nanoribbons were grown on the Al_2O_3 substrates. A small piece from the substrate was cut out for the EDS study. The spectrum was obtained by taking the data at several different points of the nanoribbon for 60 minutes. Al and O peaks in the spectrum are from the Al_2O_3 substrate. There are no other prominent peaks observed in the EDs study. From the quantitative analysis, we obtain the atomic ratio Ag:Te = 2.02:1 for the nanowire. The inset of (a): Ag/Te molar ratio of nanoribbons obtained in different batch of growth. The molar ratio is about 2.02 for the 5 samples of different batch of growth. There were no samples found with significant deviation from this ratio. (b) AFM image of a Ag_2Te nanoribbon. To use freestanding nanoribbons for the AFM, we sonicated nanoribbons grown on the Al_2O_3 substrates into the IPA solution, subsequently dripping the IPA solution to the SiO_2 substrate. Samples used for the AFM scanning vary in the thickness up to 200 nm. No samples were found to have larger thicknesses. The nanoribbons exhibit uniform surfaces. Some large nanoribbons have steps as shown in Fig. 3(b).

Photolithography was used to pattern electrodes on the nanoribbons. Cr/Au (5 nm/120 nm) contacts were deposited in a magnetron sputtering system with a base pressure of 1×10^{-8} torr. Standard DC (for large nanoribbons) and lock-in technique (for thin nanoribbons) were employed to perform four-terminal magnetoresistance measurements in a 9 Tesla Quantum Design PPMS system.

The magnetoresistance and back-gating electric effect measurement results of β-Ag_2Te are presented in this paper. As the cross section areas of samples are important for the explanation of experiment results, the width and thickness of nanoribbons are measured using scanning electron microscopy (SEM) and atomic force microscopy (AFM), respectively. As shown in Fig. 3(b), the nanoribbons exhibit uniform surfaces. Samples used for the AFM scanning vary in the thickness up to 200 nm. No samples were found to have larger thicknesses. Some nanoribbons have steps as shown in Fig. 3(b). Fig. 4(a) shows the schematic diagram of the standard four point measurements used in our experiments. Fig. 4(b) shows a scanning electron microscopic image of a typical device. A device composed of a nanoribbon and six equal-distance separated gold contacts is shown in the image.

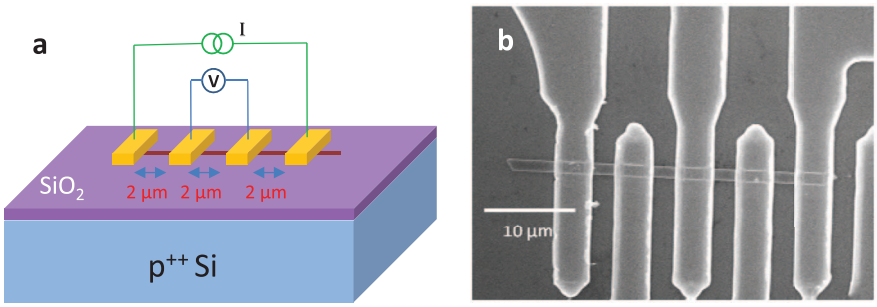

FIG. 4. (a) Schematic diagram of four contact devices used in our transport experiments. (b) A scanning electron microscopy image of device in our experiments. The image shows one nanoribbon and six gold contacts on the nanoribbon.

IV. RESULTS AND DISCUSSION

A. Aharonov-Bohm (A-B) oscillation

To probe the quantum interference effect in the β-Ag_2Te nanoribbons, we measured the magnetoresistance of a sample (cross section area: 0.191 width (W) $\times$ 0.098 thickness (T) μm^2) with the applied magnetic field parallel to the current flowing direction as shown in the schematic diagram (the inset of Fig. 5(b)). As shown in Fig. 5(a) and 5(b), pronounced and reproducible resistance oscillations with a period of 0.227 Tesla are observed at 2 K, 4 K, 6 K, 8 K and 10 K. It should be emphasized that the curves shown in 5(a) are "raw" data of resistance *vs*. magnetic field. The curves are shifted vertically for clarity and therefore have no unit for y-axis. No background subtraction is performed. The 2 K magnetoresistance in Fig. 5(a) is plotted again in Fig. 5(b) in the unit of $m\Omega \cdot cm$ for y-axis in a wider range of field from 0 Tesla to 9 Tesla. The oscillation amplitude at 2 K is about 1.5% of the total resistance. As indicated by the arrows in Fig. 5(a) and 5(b) and the FFT intensity as shown in Fig. 5(c), there are also oscillations with a period of 0.113 Tesla overlapped on the oscillations with the period of 0.227 Tesla. At 2 K, the measurements were performed with a magnetic field ramping from 0 to 9 Tesla and then ramping back from 9 to 0 Tesla. At other temperatures, the measurements were carried out up to 2.5 Tesla. It is found with no surprise that the sweeping direction has no effect on the resistance oscillations. This kind of periodic magnetoresistance oscillation can only be induced by quantum interference Aharonov-Bohm (A-B) effect or Altshuler-Aronov-Spivak (AAS) effect. As the cross section of the nanoribbon under measurement is S = thickness (98 nm) $\times$ width (191 nm), the corresponding A-B and AAS oscillation periods should be 0.221 Tesla and 0.110 Tesla, respectively. Considering the experimental error bar, we can therefore conclude that the oscillations in our measurements are attributed to a combination of A-B effect and AAS effect. Prior to the work herein, the A-B oscillation was observed in Bi_2Se_3 and Bi_2Te_3, which was regarded as one of the straightforward evidences for topological insulators.[37–39] The observation of A-B oscillations with a period of h/e unambiguously suggests the existence of conducting surface states in Ag_2Te nanoribbons, and the existence of conducting surface states on all the crystalline orientations (top, bottom and sides) provides explicit evidences for the topological origin of the surface states as expected by a topological insulator. The topological trivial surface states usually show an AAS oscillation strongly depending on the surface orientation due to bonding orientation. The existence of the A-B effect (period of h/e) at low temperature is a fingerprint of topological surface states with weak disorder, which is related to the Dirac type Hamiltonian of the helical surface state.

Recent theoretical simulations[40,41] proposed that the disorder and the Fermi level position can determine the oscillation period and whether the resistance has a minimum or maximum at zero flux. The conditions of showing A-B oscillation (h/e) or AAS oscillation (h/2e) in topological insulator nanoribbons are summarized below,

1. If a topological insulator ribbon is perfect (without disorder and doping), the transport is ballistic and the magnetotransport oscillations show a period of h/e (the A-B effect).

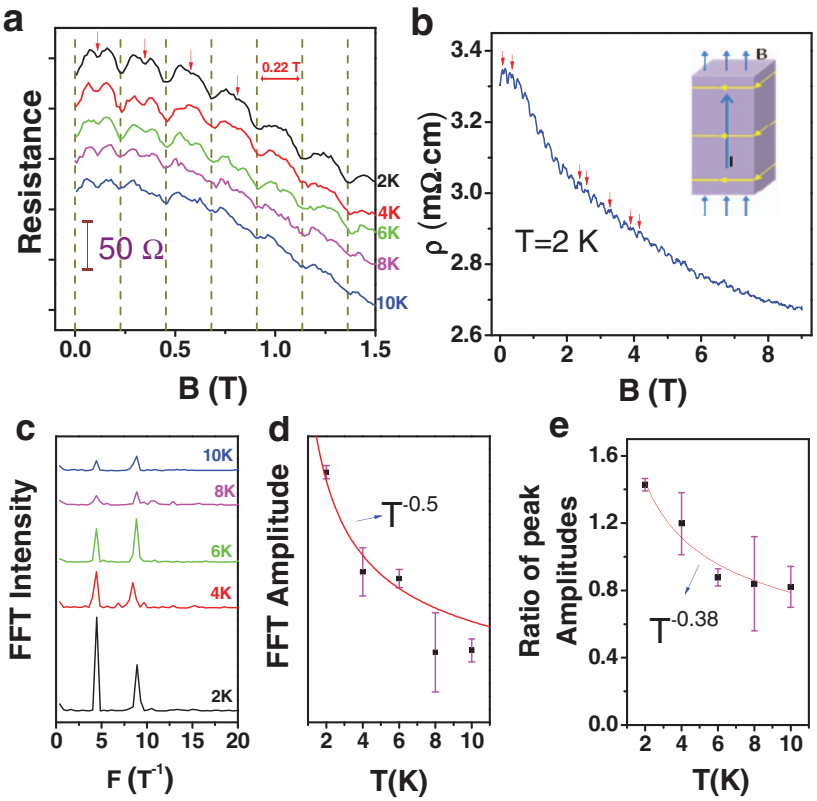

FIG. 5. (a) Magnetoresistance of a β-Ag_2Te nanoribbon (cross section area: 0.191 width (W) $\times$ 0.098 thickness (T) μm^2) with an applied magnetic field parallel to the current flowing direction at temperature 2 K, 4 K, 6 K, 8 K, and 10 K, respectively. The curves are vertically displaced for clarity. A clear resistance oscillation with a period of 0.227 Tesla (h/e) is observed, as shown by the dotted lines. The arrows indicate an oscillation with a period of 0.113 Tesla (h/2e). (b) The plot of the 2 K magnetoresistance in (a) in a wider field range from 0 Tesla to 9 Tesla. The arrow indicates the minimums of the oscillations with a period of h/2e. Inset shows the schematic diagram of the measurements. (c) The temperature dependence of the FFT spectra of the quantum oscillations. Locations of h/e and h/2e flux quantization are labeled. (d) The temperature dependence of the FFT amplitude of the h/e flux quantization (the A-B effect). The solid line is the curve of the $T^{-0.5}$ power law. (e) The ratio of the amplitude of two FFT peaks (A(h/e)/A(h/2e) at different temperatures. The power law fitting gives $\sim T^{-0.38}$.

2. If the Fermi level passes through the Dirac point of a topological insulator nanoribbon, the oscillations always show a period of h/e (the A-B effect) at any disorder strength.
3. The Fermi level is away from the Dirac point of a topological insulator nanowire. When the electron transport evolves gradually from ballistic to diffusive with increasing disorder, the quantum oscillations in a topological insulator nanoribbon show a gradual transition from a period of h/e (the A-B effect) at weak disorder to a period of h/2e (the AAS effect) at strong enough disorder simultaneously.

For a nanoribbon with trivial surface states, the period of oscillation is h/2e (the AAS effect), which is a well known knowledge in quantum transport.[45] Therefore, if the oscillation period is h/2e (the AAS effect), we can conclude that the nanoribbon has a trivial surface state or a doped topological surface state with strong disorder. If the oscillation is h/e (the A-B effect), we can conclude that the nanoribbon has a topological surface state. The topological surface state showing the A-B effect can be one of the three conditions, 1. without disorder for any doping, 2. without doping (the Fermi level passing through the Dirac point) for any disorder strength, 3. with weak disorder. Hence, the h/e oscillation in our experiment confirms the existence of topological surface state. Based on the theoretical analysis and our experimental results, we speculate that our Ag_2Te nanoribbon has a mediate disorder, and therefore exhibit oscillations with both h/e and h/2e periods.

The other possibility is that the surface state includes a dominating topological nontrivial part and a weak topological trivial part coming from band bending at the surface, which shows A-B oscillations with a period of h/e and AAS oscillation with a period of h/2e, respectively.

Recently, quantum oscillations with a period of h/e were observed in InN nanowires, which have a topological trivial surface state due to band bending.[42] However, the oscillations are caused by energy level splitting and therefore their magnitude does not decay with increasing magnetic field. The magnitude of oscillations for Ag_2Te decays with increasing magnetic field, which is a standard characteristic of quantum interference induced oscillation. Therefore, the A-B oscillation (h/e period) in our measurements should be a fingerprint of topological surface state and not be the type of oscillations in InN nanowire. The decaying speed of A-B or AAS oscillation with increasing magnetic field is related to the thickness of the surface states. The decay of the oscillation magnitude with increasing magnetic field in Ag_2Te is faster than that in Bi_2Se_3, which may indicate thicker surface states in Ag_2Te_3. To study the evolution of the A-B and AAS oscillation with increasing temperature, fast Fourier transform (FFT) was employed to analyze the derivative dR/dB. The FFT intensity of 2 K, 4 K, 6 K, 8 K, and 10 K are plotted in Fig. 5(c), which clearly shows the coexistence of the A-B oscillation (h/e) and the AAS oscillation (h/2e). As shown in Fig. 5(e), the ratio of the FFT intensity of the A-B oscillation and AAS oscillation decreases with increasing temperature, which is larger than 1 at 2 K and 4 K and smaller than 1 at 6 K, 8 K, and 10 K. This phenomenon may be explained by the increasing electron and phonon scattering with increasing temperature. As aforementioned, when the electron transport evolves gradually from ballistic to diffusive with increasing disorder or scattering, the quantum oscillation in topological insulator will show a gradual transition from h/e period (the A-B effect) to h/2e period (the AAS effect) simultaneously. Therefore, the ratio of the FFT intensity of the h/e and h/2e oscillation should decrease with increasing temperature due to the increasing scattering. The power law fitting of the temperature dependent ratio gives $\sim T^{-0.38}$.

Due to the topological surface transport, β-Ag_2Te nanoribbons actually form a two dimensional transport system. In a two dimensional electron system with high density electrons and weak electron-electron interaction, the phase coherence time $\tau_\phi \sim h/k_BT$ can be estimated from the thermal broadening of the Fermi-Dirac distribution. The oscillation amplitude is proportional to the phase coherence length $L_\phi = (D\tau_\phi)^{-1/2} \sim T^{-1/2}$. In a realistic system, the impurity scattering and phonon scattering can also affect the evolution of the phase coherence with temperature. At very low temperature regime, the scattering due to paramagnetic impurity limits the increase of L_ϕ with decreasing temperature and therefore generates a saturation behavior of L_ϕ (T). At high temperature regime, the contribution of phonon scattering induces a faster decay of L_ϕ with increasing temperature than the $T^{-1/2}$ law. The temperature dependence of oscillation amplitude of the A-B oscillation in Bi_2Se_3 and Bi_2Te_3 nanowires shows a $\sim T^{-1/2}$ power law behavior from 2 K to 20 K,[37,38] which indicates that the electron-electron interaction is dominated in the temperature regime in their samples. In the A-B effect of Bi_2Te_3 nanoflake,[39] the decay of oscillation with increasing temperature is faster than the $T^{-1/2}$ power law. As shown in Fig. 5(d), the decay of the FFT amplitude with increasing temperature of the β-Ag_2Te sample is compared with the $T^{-1/2}$ power law between 2 K and 10 K. There is no sign of saturation at 2 K, which shows that the impurity scattering effect is still negligible at this temperature. This may indicate the high quality of our sample. At 8 K and 10 K, it can be observed that the FFT amplitudes start deviating from the $T^{-1/2}$ law. The faster decay of FFT amplitude at 8 K and 10 K indicates the effect of inelastic phonon scattering. As the temperature dependence of the FFT amplitudes of the quantum oscillations of Bi_2Se_3 and Bi_2Te_3 nanowires agrees with the $T^{-1/2}$ power law up to 20 K, we may conclude that the phonon scattering effect is stronger in β-Ag_2Te nanoribbons than that in Bi_2Se_3 and Bi_2Te_3 nanowires.

B. Ambipolar electric gate effect

For a nanoribbon with topological surface states composed of Dirac cone, an ambipolar electric field effect with a sharp charge neutrality point should be expected. Pronounced ambipolar electric field effect was observed in back-gated device fabricated by a 112 nm thick β-Ag_2Te nanoribbon.

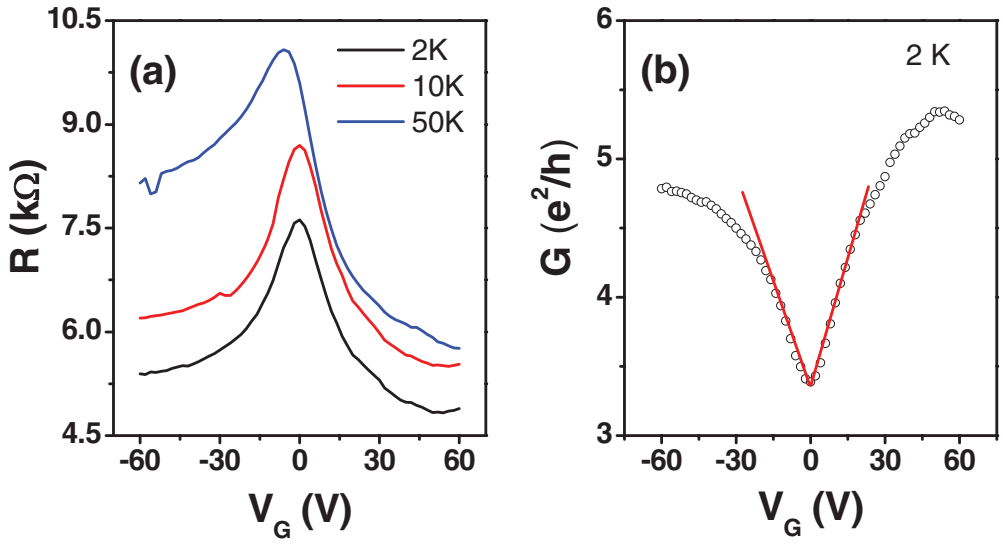

FIG. 6. (a) V_G dependence of resistance at 2 K, 10 K and 50 K, respectively. (b) V_G dependence of Conductance at 2 K. It shows quasi-linear behavior near the minimum conductance.

Fig. 6(a) shows the back gating voltage dependent resistance curves at 2 K, 10 K, and 50 K, respectively. The gating effect is negligible when T > 200 K. The sharp transition at highest resistance point (the charge neutrality point) and the gradual change of resistance when the gate voltage deviates from the charge neutrality point indicate that the ambipolar behavior may be due to a Dirac cone type topological surface state. A topologically trivial surface states induced by band bending usually generates a constant highest resistance region when the Fermi level in the gap and a dramatic decrease of resistance when the Fermi level enters into the conduction band or valence band. As shown in Fig. 6(b), the sample conductance shows a quasi-linear dependence on the gating voltage in the $-20\ V < V_G < 20\ V$ regime, which also supports the topological Dirac cone origin of the surface state. It should be noted that the ambipolar electric gate effect can also be realized in semimetals or semiconductors with very narrow band gap. Although the quasi-linear gate voltage dependent conductance usually can only be observed in materials with Dirac cone surface states, we cannot fully rule out this possibility based on the current experimental results, because the possible impurity levels in the gap of β-Ag_2Te due to defects may change the narrow band semiconductor into semimetal. The resistance of the nanoribbon can change ~35%–~40% with −60 V to 60 V gating voltage, which is a reasonable value because we can only tune the Fermi level of the bottom surface. We also observed that the highest resistance point can shift to −50 V in a time scale of several days, which may indicate the doping effect of ambient gas to the surface states. Based on the existence of topological surface state, we also successfully explained the relationship between the shape of R(T) curves and sample thickness as shown below.

C. The shape of R(T) curves *vs.* cross section areas

To further study the effect of topological surface state in electron transport, we also measured the temperature dependence of resistivity of β-Ag_2Te single crystalline nanoribbons with various cross sections to find the relationship between the resistivity and cross section area. For topological insulators with the same chemical composition, due to the surface states, the resistivity should decrease with decreasing cross section at low temperatures, which has been reported in our measurements on $Bi_{1.5}Sb_{0.5}Se_{1.8}Te_{1.2}$ bulk single crystals and nanoflake devices.[44] However, we cannot figure out a clear relationship of this kind in our measurements for β-Ag_2Te nanoribbons. We believe that this is caused by the small composition variation for different samples, which is a common problem for the CVD grown nanostructures, although the atomic ratio of Ag/Te determined by EDS is always very

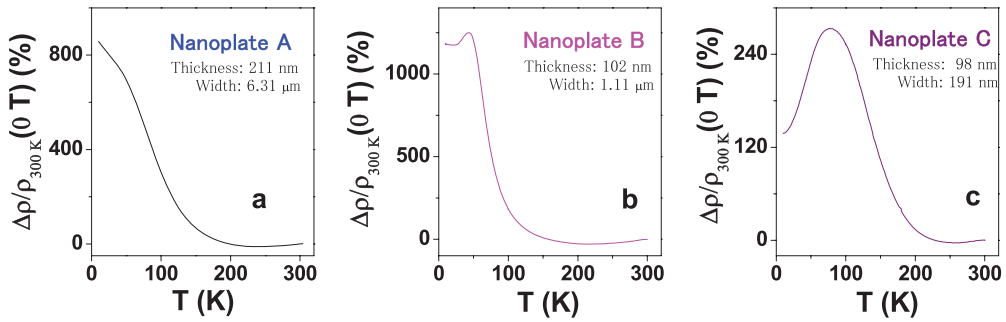

FIG. 7. The temperature dependence of normalized resistance ($\Delta\rho = \rho$ (T) $- \rho$ (300 K)) at zero magnetic field of (a) sample A, (b) sample B and (c) sample C, respectively.

near 2 for all the nanoribbons measured. As β-Ag_2Te is a narrow band semiconductor, slight composition change may generate different resistivity. The resistivity of our samples at 10 K with zero field varies from several m$\Omega \cdot$cm to thirty m$\Omega \cdot$cm. Although there is no clear relationship between the resistivity and the area of the cross-section of samples, the shape of the resistivity *vs*. temperature curves does connect with the cross-section area of nanoribbons. The temperature dependence of normalized resistance of three β-Ag_2Te nanoribbons (A, B and C) with different cross-section area is shown in Fig. 7(a)–7(c). The cross section areas of sample A, B and C are 6.31 width (W) $\times$ 0.211 thickness (T) μm^2, 1.11(W) $\times$ 0.102 (T) μm^2 and 0.191(W) $\times$ 0.098(T) μm^2, respectively. The three samples are prepared in one batch of growth. Sample A (the sample with the largest cross section area), shows semiconductor behavior in the measured temperature from 300 K to 10 K while both sample B and sample C show semiconductor characteristics at a high temperature region and present a semiconductor-to-metal transition at 50 K and 75 K, respectively. Sample C is also used for the A-B effect measurements (Fig. 5), which has the smallest cross section area. The decrease of the resistance with decreasing temperature is more pronounced in sample C comparing with that in sample B. As the A-B oscillation and ambipolar electric field effect suggests the existence of topological surface states on β-Ag_2Te, it is very natural to use the conducting surface states to account for the size dependence of electrical transport behaviors. Since the transport contribution from the metallic surface increases with decreasing size of the sample, the metallic transport characteristic starts at higher temperatures and is more pronounced at a low temperature region.

V. CONCLUSION

In conclusion, our first-principle calculations indicate the anisotropic topological surface state in β-Ag_2Te. Pronounced A-B oscillations and weak AAS oscillations are observed in the magnetoresistance measurements with the magnetic field applied along the current flowing direction in a single crystalline β-Ag_2T nanoribbon, which provides an experimental evidence for the existence of the topological surface state. The ambipolar electric field effect provides further evidence of the topological surface states in β-Ag_2Te. The size dependence of the shape resistance vs. temperature curves also can be clarified by the existence of topological surface state. The experimental evidences of topological surface states and the theoretically predicted anisotropic Dirac cone suggest that β-Ag_2Te may be a promising candidate of topological insulator for fundamental research and future spintronic devices.

NOTED ADDED

The paper has been uploaded to arXiv:1204.3816 since April 2012. In the procedure of trying to publish this paper, we noticed that a similar work[46] published recently.

ACKNOWLEDGMENT

L. W. acknowledges the support from Singapore National Research Foundation (RCA-08/018) and MOE Tier 2 (MOE2010-T2-2-059). S. Q. S. thanks the Research Grant Council of Hong Kong under Grant No. HKU705110P. W. G. Z. acknowledges the Singapore A*STAR SERC 102 101 0019. T. Y. acknowledges NTU-SUG M4080513. The authors thank Hongming Weng and Sergey V. Eremeev for their helpful discussion.

[1] J. E. Moore, Nature (London) **464**, 194 (2010).
[2] M. Z. Hasan and C. L. Kane, Rev. Mod. Phys. **82**, 3045 (2010).
[3] X. L. Qi and S. C. Zhang, Rev. Mod. Phys. **83**, 1057 (2011).
[4] M. Konig, H. Buhmann, L. W. Molenkamp, T. L. Hughes, C. X. Liu, X. L. Qi, and S. C. Zhang, J. Phys. Soc. Jpn. **77**, 031007 (2008).
[5] M. Konig, S. Wiedmann, C. Brune, A. Roth, H. Buhmann, L. W. Molenkamp, X. L. Qi, and S. C. Zhang, Science **318**, 766 (2007).
[6] I. Knez, R. R. Du and G. Sullivan, Phys. Rev. Lett. **107**, 136603 (2011).
[7] J. N. Hancock, J. L. M. van Mechelen, A. B. Kuzmenko, D. van der Marel, C. Brune, E. G. Novik, G. B. Astakhov, H. Buhmann, and L. W. Molenkamp, Phys. Rev. Lett. **107**, 136803 (2011).
[8] C. Brune, C. X. Liu, E. G. Novik, E. M. Hankiewicz, H. Buhmann, Y. L. Chen, X. L. Qi, Z. X. Shen, S. C. Zhang, and L. W. Molenkamp, Phys. Rev. Lett. **106**, 126803 (2011).
[9] Y. Xia, D. Dian, D. Hsieh, L. Wray, A. Pal, H. Lin, A. Bansil, D. Grauer, Y. S. Hor, R. J. Cava, and M. Z. Hasan, Nat. Phys. **5**, 398 (2009).
[10] Y. L. Chen, J. G. Analytis, J. H. Chu, Z. K. Liu, S. K. Mo, X. L. Qi, H. J. Zhang, D. H. Lu, X. Dai, Z. Fang, S. C. Zhang, I. R. Fisher, Z. Hussain, and Z. X. Shen, Science **325**, 178 (2009).
[11] D. Hsieh, Y. Xia, L. Wray, D. Qian, A. Pal, J. H. Dil, J. Osterwalder, F. Meier, G. Bihlmayer, C. L. Kane, Y. S. Hor, R. J. Cava, and M. Z. Hasan, Science **323**, 919 (2009).
[12] D. Hsieh, Y. Xia, D. Qian, L. Wray, J. H. Dil, F. Meier, J. Osterwalder, L. Patthey, J. G. Checkelsky, N. P. Ong, A. V. Fedorov, H. Lin, A. Bansil, D. Grauer, Y. S. Hor, R. J. Cava, and M. Z. Hasan, Nature (London) **460**, 1101 (2009).
[13] J. G. Analytis, J. H. Chu, Y. Chen, F. Corredor, R. D. McDonald, Z. X. Shen, and I. R. Fisher, Phys.Rev. B **81**, 205407 (2010).
[14] Y. S. Hor, A. Richardella, P. Roushan, Y. Xia, J. G. Checkelsky, A. Yazdani, M. Z. Hasan, N. P. Ong, and R. J. Cava, Phys. Rev. B **79**, 195208 (2009).
[15] J. G. Checkelsky, Y. S. Hor, R. J. Cava, and N. P. Ong, Phys. Rev. Lett. **106**, 196801 (2011).
[16] N. P. Butch, K. Kirshenbaum, P. Syers, A. B. Sushkov, G. S. Jenkins, H. D. Drew, and J. Paglione, Phys. Rev. B **81**, 241301(R) (2010).
[17] J. Chen, H. J. Qin, F. Yang, J. Liu, T. Guan, F. M. Qu, G. H. Zhang, J. R. Shi, X. C. Xie, C. L. Yang, K. H. Wu, Y. Q. Li, and L. Lu, Phys. Rev. Lett. **105**, 176602 (2010).
[18] H. T. He, G. Wang, T. Zhang, I. K. Sou, G. K. L. Wong, J. N. Wang, H. Z. Lu, S. Q. Shen, and F. C. Zhang, Phys. Rev. Lett. **106**, 166805 (2011).
[19] S. Matsuo, T. Koyama, K. Shimamura, T. Arakawa, Y. Nishihara, D. Chiba, K. Kobayashi, T. Ono, C. Z. Chang, K. He, X. C. Ma, and Q. K. Xue, Phys. Rev. B **85**, 075440 (2012).
[20] J. Wang, A. M. DaSilva, C. Z. Chang, K. He, J. K. Jain, N. Samarth, X. C. Ma, Q. K. Xue, and M. H. W. Chan, Phys. Rev. B **83**, 245438 (2011).
[21] R. Xu, A. Husmann, T. F. Rosenbaum, M. L. Saboungi, J. E. Enderby, and P. B. Littlewood, Nature (London) **390**, 57 (1997).
[22] A. Husmann, J. B. Betts, G. S. Boebinger, A. Migliori, T. F. Rosenbaum, and Saboungi M. L., Nature (London) **417**, 421 (2002).
[23] A. A. Abrikosov, Phys. Rev. B **58**, 2788 (1998).
[24] M. M. Parish and P. B. Littlewood, Nature (London) **426**, 162 (2003).
[25] J. S. Hu and T. F. Rosenbaum, Nat. Mater. **7**, 697–700 (2008).
[26] W. Zhang, R. Yu, W. X. Feng, Y. G. Yao, H. M. Weng, X. Dai, and Z. Fang, Phys. Rev. Lett. **106**, 156808 (2011).
[27] V. E. Sackstedar IV, S. Kettemann, X. Dai, Q. S. Wu, and Z. Fang, arXiv:1108.2938v1 (2011).
[28] G. Kresse and J. Hafner, Phys. Rev. B **48**, 13115 (1993).
[29] P. E. Blochl, Phys. Rev. B **50**, 17953–17979 (1994).
[30] J. P. Perdew, K. Burke, and M. Ernzerhof, Phys. Rev. Lett. **77**, 3865–3868 (1996).
[31] D. D. Koelling and B. N. Harmon, J. Phys. C: Solid Stat. Phys. **10**, 3107 (1977).
[32] A. van der Lee and J. L. de Boer, Acta Cryst. C **49**, 1444–1446 (1993).
[33] R. Dalven, Phys. Rev. Lett. **16**, 311–312 (1966).
[34] R. Dalven and R. Gill, Phys. Rev. B **159**, 645–649 (1967).
[35] L. Fu, Phys. Rev. Lett. **103**, 266801 (2009).
[36] J. H. In, Y. D. Yoo, J. G. Kim, K. Y. Seo, H. J. Kim, H. Ihee, S. H. Oh, and B. S. Kim, Nano Lett. **10**, 4501 (2010).
[37] H. Peng, K. Lai, D. Kong, S. Meister, Y. Chen, X.-L. Qi, S.-C. Zhang, Z.-X. Shen, and Y. Cui, Nat. Mater. **9**, 225 (2010).
[38] F. X. Xiu, L. He, Y. Wang, L. Cheng, L. T. Chang, M. Lang, G. Huang, X. F. Kou, Y. Zhou, X. W. Jiang, Z. G. Chen, J. Zou, A. Shailos, and K. L. Wang, Nat. Nano. **6**, 216 (2011).
[39] Z. G. Li, Y. Y. Qin, F. Q. Song, Q. H. Wang, X. F. Wang, B. G. Wang, H. F. Ding, C. van Haesondonck, J. G. Wang, Y. H. Zhang, G. H. Wang, Appl. Phys. Lett. **100**, 083107 (2012).

[40] Y. Zhang and A. Vishwanath, Phys. Rev. Lett. **105**, 206601 (2010).
[41] J. H. Bardarson, P. W. Brouwer, and J. E. Moore, Phys. Rev. Lett. **105**, 156803 (2010).
[42] T. Richer, C. Blomers, H. Luth, R. Calarco, M. Indlekofe, M. Marso, and T. Schapers, Nano Lett. **8**, 2834 (2008).
[43] C. Y. Moon, J. H. Han, H. Lee, and H. J. Choi, Phys. Rev. B **84**, 195425 (2011).
[44] B. Xia, P. Ren, A. Sulaev, P. Liu, S.-Q. Shen, L. Wang, Phys. Rev. B **87**, 085442 (2013).
[45] V. F. Gantmakher, *Electrons and Disorder in Solids* (Oxford Science Publications, 2005).
[46] S. G. Lee, J. H. In, Y. D. Yoo, Y. G. Jo, Y. C. Park, H. J. Kim, H. C. Koo, J. Kim, B. S. Kim, and K. L. Wang, Nano Lett. **12**, 4194 (2012).